31st Annual International Conference of the IEEE EMBS
Minneapolis, Minnesota, USA, September 2-6, 2009

Large-scale integrated model is useful for understanding heart mechanisms and developments of medical therapy

Takumi Washio, Jun-ichi Okada, PhD, Seiryo Sugiura, MD, PhD, and Toshiaki Hisada, PhD

Abstract— **In this paper, we discuss the need for a large-scale integrated computer heart model to understand cardiac pathophysiology and to assist in the development of novel treatments through our experiences with the "UT-heart" simulator. The UT-heart simulator is a multi-scale, multi-physics heart simulator that integrates and visualizes our knowledge of cardiac function in various aspects and scales. To demonstrate the usefulness of this model, we focus especially on two problems in cardiac anatomy and physiology. In the first application, the mechanistic implication of complex fiber and laminar structures is analyzed with respect to optimality of pumping performance. In the second application, the coronary circulation is analyzed, to identify factors that determine the behavior of the microcirculatory system. These two examples indicate not only the importance of the integration technique, but also the need to resolve structural complexities of the heart in the modeling. This leads naturally to incorporating high performance computing in medical therapy.**

I. UT-HEART SIMULATOR

To understand fully the mechanism of the heart in its normal and diseased states, we must integrate our knowledge ranging from molecular and cellular levels to organ levels. Furthermore, the function at each level is based on a variety of disciplines including biochemistry, electricity, and solid/fluid mechanics, which necessitates the use of multi-modal experimental and diagnostic tools. In this context, we have developed a multi-scale, multi-physics heart simulator (called the UT-heart simulator [1]), which integrates and visualizes our knowledge of the cardiac functions.

The heart simulator is based on the finite element method for most of the simulations ranging from electric to mechanics phenomena, and from micro- to macroscopic phenomena. Here, we introduce the general principles of the simulation procedure for an organ level simulation using the UT-heart simulator. The morphology of the heart is taken from human multi-detector CT data and modeled together with the blood in its cavity. For the electrophysiology simulation, a composite voxel mesh with fine voxels around the heart and coarse voxels covering the torso is adopted to solve the bidomain equation [2]. Following the excitation of a sinus node, the simulator reproduces the excitation propagation and depolarization of the membrane potentials of virtual cells sequentially in the atria, conduction system, and ventricles.

The mechanical simulation including intracavitary blood flow is performed on a tetrahedral mesh. The Ca^{2+} concentration data obtained from the electrophysiology model is applied to the molecular model of sarcomere dynamics to compute the contraction force of every element. This results in the synchronous contraction of the heart and blood flow.

Thus far, we have been able to retrieve and present the data in the same way with clinical diagnostic tools, such as ECG, UCG, and magneto-cardiogram in our simulation studies. These data are in good agreement with the clinical data for both normal and diseased heart models, thus suggesting their potential for diagnostic support.

The main objective of this paper is to discuss the need for large-scale computation to resolve the spatial complexities of a human heart. In this context, we present two examples, one for the fiber and laminar structures, and the other for the coronary circulation.

II. COMPLEXITIES OF FIBER AND LAMINAR STRUCTURES

A human heart has complicated three-dimensional structures. One of the complexities is the spatial arrangement of the fiber direction, while the other is the laminar structure. In regard to the twisting fiber direction along the transmural direction, it is generally believed that the fiber angle measured in a circumferential direction decreases linearly from 60 degrees at the endocardium to -60 degrees at the epicardium. However, measurements of the fiber angles in a human heart obtained by a histological section technique [3] and by a DTMRI technique [4] indicate that the above description for the transmural change may be too simple. The data obtained in the above mentioned studies indicate non-linear dependency of angles on the wall depth, while the range of angles across the transmural line also depends on the position in the left ventricle. Thus, the question arises whether such complicated regional dependence and wall depth dependence of the fiber angle really is significant in optimizing the pumping performance or not. The fact that the shape of the left ventricle is neither completely ellipsoidal nor axisymmetrical, and that there is also a right ventricle attached, suggest the functional significance of complex fiber orientations.

Manuscript received April 7, 2009. UT-heart had been developed under an intensive research activity supported by Core Research for Evolutional Science and Technology, Japan Science and Technology Agency. UT-heart is continuously being developed under cooperation with Fujitsu Ltd. by University-Industry Collaborative Grants Fostering Innovation in Technology-Seeds, Japan Science and Technology Agency.

T. Washio and J. Okada are now with Graduate School of Frontier Sciences, The University of Tokyo, 5-1-5 Kashiwanoha, Kashiwa, Chiba, 277-0882, Japan (phone: ++81-4-7136-4668; fax: ++81-4-7136-4668; e-mail: washio@ sml.k.u-tokyo.ac.jp, okada@sml.k.u-tokyo.ac.jp).

S. Sugiura and T. Hisada are now with Graduate School of Frontier Sciences, The University of Tokyo, 7-3-1 Hongo, Bunkyo-ku, Tokyo 113-0033, Japan (e-mail: hisada@mech.t.u-tokyo.ac.jp, sugiura@k.u-tokyo.ac.jp).

The laminar (sheet) structure of a heart is identified and defined by introducing another direction, orthogonal to the fiber direction. We call this the sheet direction. As shown in the literature [5] [6], the transmural change in sheet direction depends on the location in the heart and also on the species. The mechanical role of the laminar structure remains to be clarified.

In order to answer such questions, simulation studies have been attempted [7] [8]. In this study, we performed the following sequence of simulations with the heart simulator. First, initial fiber and laminar structures were constructed according to Ref. [5] on a tetrahedral mesh consisting of 79000 elements as shown in Fig. 1. Then, an optimization process of the fiber-sheet structure using a sensitivity analysis technique of the finite element method was applied to minimize systolic intracavitary volume. Here, an appropriate contraction stress, taking into account the influence of stretch in the fiber direction, was imposed over the walls. Following the optimization in the systolic deformation, the sheet angle was optimized to maximize the diastolic volume whilst keeping the fiber angle fixed. We adopted this strategy based on the following consideration. Because, in the applied model, the active stress works only along the fiber direction, the cross-fiber anisotropy, i.e. the sheet structure, does not have significant effect on the systolic function. Accordingly, the main role of the sheet structure is to decrease the deformation energy of the muscle during the filling period.

Nevertheless, the performance of the heart was considerably improved as shown in Fig. 2 and Table I. In particular, the ejection fraction exceeded 64% with fiber shortening of 17% for the optimized structure, whereas it was 56% with fiber shortening of 16% before the optimization. This substantial improvement was attained only through the rearrangement of the fiber and sheet angles. Figures 3-4 show how these angles were modified by the optimizations at the blocks indicated in Fig. 1. Interestingly enough, the angles obtained by the optimization agree with the experimental studies with respect to the following points. (a) There are plateau sections from the midwall to the endocardium for the fiber angle [3], [4]. (b) In the anterior basal block (Block 1), a steep negative fiber angle at the epicardium is observed [3]. (c) There are two branches of the sheet angle at the endocardium [9].

From an energetic analysis using stress information obtained by the heart simulator, it appears that the optimized shallower fiber angle at the endocardium increased the work done by circumferential strain (**cc** in Fig. 5), while the optimized steeper fiber angle at the epicardium increased the work done by the longitudinal strain (**ll** in Fig. 5) and the longitudinal-radial shear strain (**lr** in Fig. 5).

In regard to the sheet angle, strong concentration of the deformation energy at the endocardium was observed at the end-diastole in the simulation model. It seems that the sheet angle bifurcation releases the deformation energy to make expansion easier at the endocardium.

The simulation studies introduced thus far demonstrate the potential of the heart simulator for promoting better understanding of the roles of the fiber and laminar structures. By exploiting finite element analysis techniques such as sensitivity analysis and stress-strain analysis, we can reveal that which experimental studies hardly observe. At the same time, the above studies suggest the need for careful data preparation of the structure when performing a simulation for a specific patient. Even with state of the art observation tools like DTMRI, it still seems difficult to obtain appropriate data for the simulation study. There is, however, the possibility of improving the data by using observation motion data, for example, obtained by the echocardiograph, or tagged MR imaging. The finite element technique will again play an important role in this process.

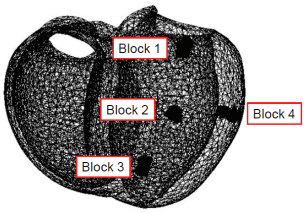

Fig. 1. The points at which the fiber and sheet angles are measured in the numerical experiments. There are 78000 tetrahedral elements in this model.

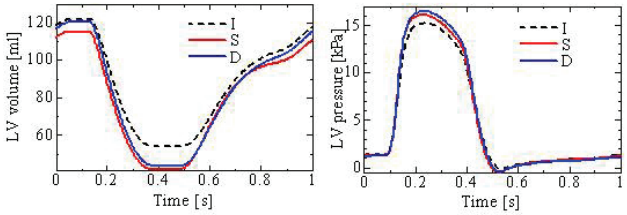

Fig. 2. Time courses of intracavitary volume and pressure of the left ventricle. I: the initial fiber-sheet structure, S: after the systolic optimization, D: after the diastolic optimization.

TABLE I

Ventricular performance with initial (I), systolic optimized (S), and diastolic optimized (D) structure. V_{max}: maximal volume, V_{min}: minimum volume, EF: ejection fraction, E_{ff} : fiber strain, C.F. : contraction force.

Case	V_{max} [ml]	V_{min} [ml]	V_{stroke} [ml]	EF [%]	E_{ff}	stretch	C.F. [kPa]
I	122.1	54.1	68.0	55.7	-0.164	0.930	39.2
S	115.4	41.6	73.8	64.0	-0.171	0.917	34.1
D	120.7	43.7	77.0	63.8	-0.170	0.925	34.5

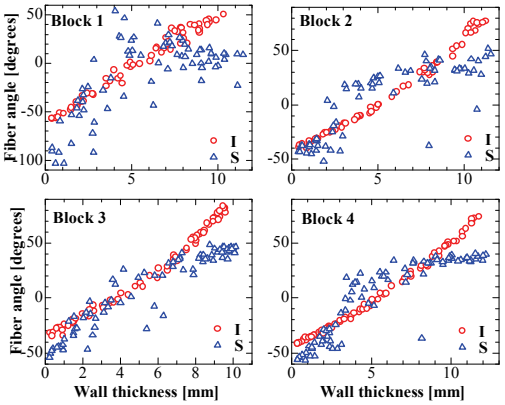

Fig. 3. Fiber angles for I (circles): the initial structure and S (triangles): after the systolic optimization. In the wall thickness indication, zero corresponds to the epicardium.

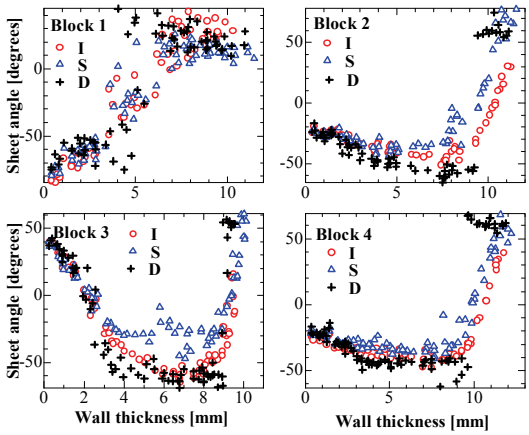

Fig. 4. Sheet angles for I (circles): the initial structure, S (triangles): after the systolic optimization and D (pluses) after the diastolic optimization. In the wall thickness indication, zero corresponds to the epicardium.

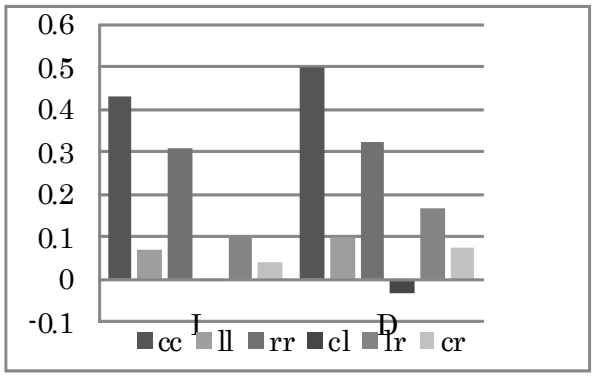

Fig. 5. Work components of the total work over the left ventricle for a single beat. The unit of work is J. The total work for I (the initial structure) is 0.95 J and for D (after the diastolic optimization) 1.13 J.

III. Coronary Circulation Analysis

One of the interesting topics, not only for basic research but also for clinical setting, is coronary circulation.

The UT-heart simulator can simulate the interaction between the contraction of the wall and the coronary circulation based on the model depicted in Fig. 6. Here, the microcirculatory system is assumed to have different capacitors in the three layers comprising the small artery, the capillary and the small vein. The blood stored in the capacitors is determined by the pressure differences between the vessels and the wall. The governing equations for the microcirculatory system and the wall are given by:

$$\rho \ddot{\mathbf{u}} = \nabla \cdot (\boldsymbol{\sigma} - p\mathbf{I}) \qquad (1)$$

$$-(J-1) + \sum_{\alpha} c_{\alpha}(\mu_{\alpha} - p) = 0 \qquad (2)$$

$$\nabla(\kappa_{\alpha} \nabla \mu_{\alpha}) - c_{\alpha}\left(\frac{d\mu_{\alpha}}{dt} - \frac{dp}{dt}\right) + Z_{\alpha} = 0 \qquad (3)$$

Here, the microcirculatory system is modeled as a continuum model since it cannot be resolved in the scale of the finite element mesh. Eq. (1) is the equation of motion for the wall where p is the hydrostatic pressure. Eq. (2) represents the volume balance where J is the volume rate of the wall compared with the unstressed state, and the second term is the increase of blood in the capacitors. Here, the index α indicates the layer (small artery, capillary or small vein), and μ_{α} is the pressure inside the vessel. The variable c_{α} is the capacitance per unit volume, not only for the vessels but including the muscle surrounding them. Eq. (3) represents the balance of flux at each point in the wall, where Z_{α} is the flux from the other parts in the circulatory system. The first diffusive term on the left hand side represents the flow in the capillary network. This term is applied only to the capillary layer as depicted by the horizontal broken line in the rightmost diagram of Fig. 6.

The arterial and venous networks out of the microcirculatory system were constructed by following the statistical data in [10], [11]. The resultant networks are shown in Fig. 7. There are 49000 and 47000 pipes representing the arterial and venous networks, respectively. The structure mesh on the ventricular wall and the fluid mesh in the cavities consist of 410000 and 390000 tetrahedral elements, respectively. The vessel conductance in the networks was determined from its diameter according to Poiseuille's law. Depicted in Fig. 8 are the temporal changes in the pressures and the total coronary flows obtained by the simulation. Typical time profiles for the arterial and venous flows were reproduced correctly. The total inflow to the coronary was 151[ml/min] which agrees well with the experimental study.

The flow pattern in the microcirculatory system is shown in Fig. 9. As confirmed in the literature [12], a strong reverse flow in early systole and a weaker reverse flow during late systole were obtained in the subendocardial small artery. It appears that this strong reverse flow is basically due to the singular behavior of the time derivative dp/dt of the hydrostatic pressure in Eq. (3). Moreover, the singular behavior of dp/dt originates from the dependence of the contraction force on the stretch velocity which is modeled with the fading memory model [13] in the UT-heart simulator. On the other hand, it is also shown in the rightmost diagram of Fig. 9 that the temporal change in flux around the capillary is relatively mild since the noise was filtered by the CR (capacitor-resister) circuit function.

As seen here, to understand the mechanism of coronary circulation, we need to take several factors into account, namely the coronary network structure, spatial and temporal change in the hydrostatic pressure, characteristics of the contractile force, etc. This once again indicates the need for a correct modeling of the heart structure in an appropriate spatial resolution. As a further application of the UT-heart simulator, studies of coronary stenoses were attempted. For example, in Fig. 10, the fluxes downstream of a stenotic part are compared with the control. Here, two cases were simulated. In the first case, only the vessel conductance at the stenotic part was modified, while in the second case, the contractility in the region downstream of the stenotic part was also reduced according to the decrease in blood supply. In the second case, dominancy of the flow in the systolic phase was strengthened as was expected.

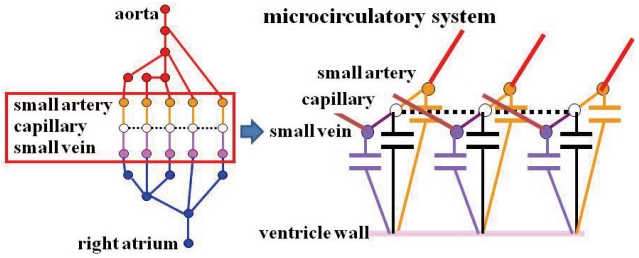

Fig. 6. Coronary circulation model in UT-heart simulator. Basic concepts of the total coronary system (left) and of the microcirculatory system (right).

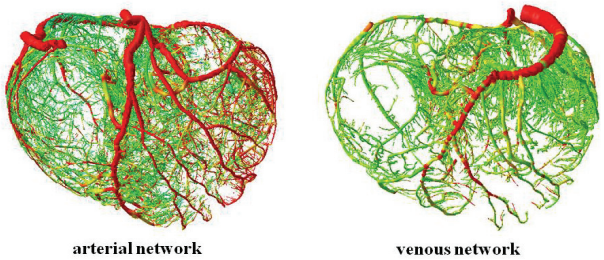

Fig. 7. Arterial (left) and venous (right) networks out of the microcirculatory system (These pictures were provided by Dr. M. Watanabe, Fujitsu Ltd.).

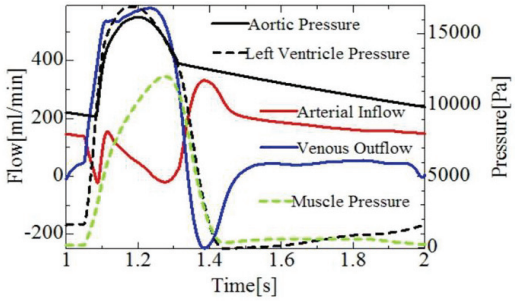

Fig. 8. Temporal changes in the pressures and the total coronary flows.

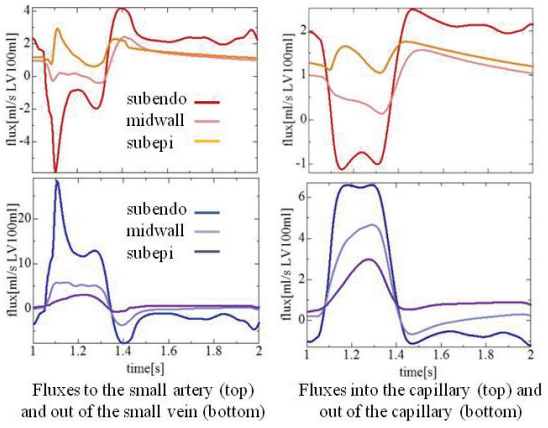

Fig. 9. Temporal change in fluxes in the microcirculatory system at the subendocardium (subendo), the midwall and the subepicardium (subepi) at the lateral equator of the left ventricle. On the left, the flux to the small artery from the arterial network and the flux out of the small vein to the venous network are shown. On the right, the flux from the small artery to the capillary and the flux out of the capillary to the small vein are shown.

IV. CONCLUSION

Through the two application examples of the UT-heart simulator, we demonstrated the usefulness of large-scale computation to promote understanding of the heart mechanism. We also showed the possibility of applying computing technology to solving the problems of ischemia.

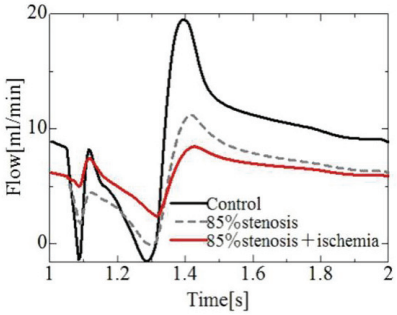

Fig. 10. Comparison of the fluxes downstream of the stenotic part. In the case of "stenosis", only the vessel diameter of the stenotic part is reduced by 85 percent, whereas in the case of "stenosis+ischemia", the contractile ability is also reduced according to the blood supply over the downstream region.

Next we intend combining a model of the metabolic system with the coronary simulator targeting utilization of the UT-heart simulator for clinical practice. Through such activities, we aim to open doors for applying computational science and technologies in new medical applications.

REFERENCES

[1] http://www.sml.k.u-tokyo.ac.jp/

[2] T. Washio, J. Okada and T. Hisada, "A parallel multilevel technique for solving the biodomain equation on a human heart with Purkinje fibers and a torso model", *SIAM Journal on Scientific Computing*, vol. 30, No. 6, pp. 2855–2881, 2008.

[3] R.A. Greenbaum, S.Y. Ho, D.G. Gibson, A.E. Becker and R.H. Anderson, "Left ventricular fibre architecture in man", *Br. Heart J*, vol. 45, pp. 248–263, 1981.

[4] D. Rohmer, A. Sitek, and G.T. Gullberg, "Reconstruction and visualization of fiber and laminar structure in the normal human heart from ex vivo diffusion tensor magnetic resonance imaging (DTMRI) data", *Investigation Radiology*, vol. 42, pp. 777–789, 2007.

[5] K.D. Costa, Y. Takayama, A.D. McCulloch and J.W. Covell, "Laminar fiber architecture and three-dimensional systolic mechanics in canine ventricular myocardium", *Am J Physiol Heart Circ Physiol*, vol. 276, pp. 595–607, 1999.

[6] I.J. LeGrice, B.H. Smaill, L.Z. Chai, S.G. Edgar, J.B. Gavin and P.J. Hunter, "Laminar structure of the heart: ventricular myocyte arrangement and connective tissue architecture in the dog", *Am J Physiol Heart Circ Physiol*, vol. 269, pp. H571–H582, 1995.

[7] F. Dorri, P.F. Niederer and P.P. Lunkenheimer, "A finite element model of the human left ventricular systole", *Computer Methods in Biomechanics and Biomedical Engineering*, vol. 9, pp.319–341, 2006.

[8] T.P. Usyk, R. Mazhari and A.D. Mcculloch, "Effect of Laminar Orthotropic Myofiber Architecture on Regional Stress and Strain in the Canine Left Ventricle", *Journal of Elasticity*, vol. 61, pp. 143–164, 2000.

[9] J.W. Covell, "Tissue structure and ventricular wall mechanics", *Circulation*, Vol. 118, pp. 699–701, 2008.

[10] G. S. Kassab, C. A. Rider, N. J. Tang and Y. C. Fung, "Morphometry of pig coronary arterial trees", *Am J Physiol Heart Circ Physiol* , vol. 265, pp. H350–H365, 1993.

[11] G. S. Kassab, D. H. Lin and Y. C. Fung, "Morphometry of pig coronary venous system", *Am J Physiol Heart Circ Physiol*, vol. 267, pp. H2100–H2113, 1994.

[12] E. Toyota, Y. Ogasawara, O. Hiramatsu, H. Tachibana, F. Kajiya, S. Yamamori and W.M. Chilian, "Dynamics of flow velocities in endocardial and epicardial coronary arterioles", *Am J Physiol Heart Circ Physiol*, vol. 288, pp. H1598–H1603, 2005.

[13] P.J. Hunter, A.D. McCulloch and H.E.D.J. ter Keurs, "Modeling the mechanical properties of cardiac muscle", *Progress in Biophysics & Molecular Biology*, vol. 69, pp. 289–331, 1998.